Numerical Simulation for Dual-energy CT Imaging

Lixin Wang[1], Fengrong Sun*[1], Paul Babyn[2], Hai Zhong[3], Zhenzhen Zhou[1], Hao Huang[1], Jiaojiao Qin[1]

[1]School of Information Science and Engineering, Shandong University, Jinan, China.

[2]Department of Medical Imaging, University of Saskatchewan and Saskatoon Health Region, Saskatoon, Canada.

[3]Radiology Department of The Second Hospital of Shandong University, Jinan, China

([*]Corresponding author: sunfr@sdu.edu.cn)

Keywords: dual-energy CT; numerical simulation; material decomposition; image reconstruction

Abstract. The clinical application of dual-energy CT (DECT) system is a significant technical progress in X-ray medical imaging for recent years. Compared with conventional CT, DECT is capable of differentiating tissue and eliminating beam hardening artifacts and plays a unique role in current diagnostic imaging. But it is not easy for the researchers to acquire DECT raw projection data. And it has become a bottleneck for those theoretical explorations on DECT imaging. We propose a method to implement the numerical simulation for the material decomposition and image reconstruction of DECT imaging, based on the physics and mathematics of CT/DECT imaging. The experimental results show the validity and the reliability of our method.

1. Introduction

Computed Tomography (CT) is a technique that can obtain the inner structure images of the scanned object with multiple X-ray projections taken at different angles. Compared with conventional CT by which we can only get the distribution of linear attenuation coefficients, dual-energy CT (DECT) is capable of elimination beam hardening artifacts and providing us with additional information about electron density and atomic number, which can be used to discriminate materials. So DECT is playing a unique role in modern diagnostic imaging.

As early as the 1970s, when the concept of DECT was first proposed by Alvarez, and quickly became a highly interesting topic in medical imaging field. But its clinical application was not so popular due to the limitation of equipment. There was no impressive technical progress for DECT until SOMATOM Definition Flash dual-source CT system was announced by Siemens in 2006, which overcomes the limitation by permitting the use of two X-ray sources at two different keV levels simultaneously [1]. GE Healthcare also released Discovery CT750 HD dual-energy CT system in RSNA 2007, which uses a single X-ray source with fast switching between two kilovoltage settings to generate high-and low-energy X-ray spectra [2].

For the theoretical research of DECT imaging technology, it is required to acquire the raw projection data sets at high- and low-energy level photon spectra. There are two ways to get such data sets. The first one obtains projection data sets via the data export interface of actual DECT system. But it is limited by intellectual property protection and insufficient technical support from manufacturers. The second one gets the raw data sets through the pseudo DECT scanning, which means a conventional CT system scans the same object two times separately with two different kVp levels of the X-ray tube voltages. But it fails to seamlessly align the imaged anatomy and to capture the same phase of contrast enhancement. So we propose a method in this paper to realize the numerical simulation for the material decomposition and image reconstruction of DECT imaging.

2. Theory and Methods

2.1 Basic physics of CT imaging

The fundamental contrast mechanism for CT is the ability of tissue to scatter or absorb X-ray photons. The behavior of this attenuation is governed by the Beer-Lambert Law. In a conventional X-ray CT system, the primary spectrum from X-ray tube is polychromatic and detectors integrate over energy, then

$$I = \int_0^{E_{\max}} S(E) e^{-\int \mu(E,x)dx} dE \tag{1}$$

where $S(E)$ denotes the system spectrum, I is the intensity past the object, $\mu(x)$ denotes the linear attenuation function along the ray path x. Then projection function is easily formulated as [3]:

$$P = -\ln \frac{I}{I_0} = \int_0^{E_{\max}} S(E) dE - \int_0^{E_{\max}} S(E) \mathrm{e}^{-\int \mu(E,x)dx} dE \tag{2}$$

where I_0 is the intensity of the source , P represents the raw projection data.

2.2 Basis material decomposition model

In the diagnostic X-ray energy range, basis material decomposition model is that the linear attenuation coefficient of a voxel at energy E can be expressed as a linear combination of two attenuation coefficient of two basis materials as below.

$$\mu(E) = \mu_1(E) \cdot b_1 + \mu_2(E) \cdot b_2 \tag{3}$$

where $\mu(E)$ denotes the linear attenuation coefficient function of a material to be decomposed, $\mu_1(E)$ and $\mu_2(E)$ denote the linear attenuation coefficient functions of the two basis materials respectively, and b_1, b_2 are decomposition coefficients.

Substitute Eq. (3) into Eq. (2), we get the following formulate:

$$P = \ln \int S(E) dE - \ln \int S(E) \exp\left[-B_1 \mu_1(E) - B_2 \mu_2(E)\right] dE \tag{4}$$

where B_1 and B_2 are called basis material decomposition projections and

$$B_1 = \int b_1 dl \quad , \quad B_2 = \int b_2 dl \tag{5}$$

In a dual energy scanning mode, two measurements are taken for each ray path are as follows:

$$\begin{cases} P_H = \ln \int S_H(E) dE - \ln \int S_H(E) \exp\left[-B_1 \mu_1(E) - B_2 \mu_2(E)\right] dE \\ P_L = \ln \int S_L(E) dE - \ln \int S_L(E) \exp\left[-B_1 \mu_1(E) - B_2 \mu_2(E)\right] dE \end{cases} \tag{6}$$

where P_H, P_L denote the projection data sets under high-and low-energy spectrum. The basic task is to estimate b_1, b_2 as accurately as possible for each volume element.

2.3 Simulation steps

The steps of our numerical simulation method are specified as follows.

(1) Get X-ray spectrum of 80/140kVp from open source program Spectrum GUI [4] and divide them into n discrete intervals: $E_1, E_2, \cdots, E_n$

(2) Generate synthetic projection data by the following discrete projection function:

$$P = \sum_{i=1}^{n} \mu(E_i) \cdot \tilde{N}_i \cdot l \quad , \quad \tilde{N}_i = \frac{N_i}{\sum_{k=1}^{n} N_k} \tag{7}$$

where N_i represents the number of photons of the ith energy interval, $\mu(E_i)$ denotes the linear attenuation coefficient function at energy E.

(3) Plug Eq. (3) into Eq. (7), the projection functions at high-and low-energy spectrum are

$$\begin{cases} P_H = B_1 \cdot \mu_{1H}(E) + B_2 \cdot \mu_{2H}(E) \\ P_L = B_1 \cdot \mu_{1L}(E) + B_2 \cdot \mu_{2L}(E) \end{cases} \quad (8)$$

(4) Solve linear equations Eq. (8) and obtain the decomposition projections B_1, B_2.

(5) Get decomposition coefficients b_1, b_2 and reconstruct basis material density images.

(6) Yield a set of monochromatic images by changing the value of E in Eq. (3).

(7) Reconstruct the electron density image according to the formula:

$$\rho_e = \rho_{e1} \cdot b_1 + \rho_{e2} \cdot b_2 \quad (9)$$

where ρ_{e1} and ρ_{e2} are electron density of basis materials which can be obtained from NIST standard reference database [5].

(8) Reconstruct the effective atomic number image by employing the monochromatic attenuation ratio method [6], since the monochromatic attenuation ratio is a monotonic as a function of effective atomic number as below:

$$Z_{eff} = f(\mu(E_1)/\mu(E_2)) \quad (10)$$

where $E_1 = 70kev$ and $E_2 = 120kev$. So we can plot the effective atomic number as a function of $\mu(E)$ at two energies and compute Z_{eff}.

3. Experiments and Results

We employ here a modified version of Shepp-Logan head phantom that demonstrated in Figure 1 contains three ellipses with different absorption properties. The part of No.1 is filled with 6.67% diluted iodine which represents the iodine contrast medium; the part of No.2 is filled with tissue-equivalent plastic A-150 which represents the human tissue; and the part of No.3 is filled with bone-equivalent plastic B-100 which represents the human bone.

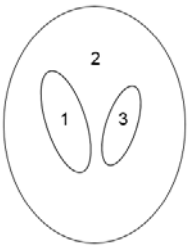

Fig.1 Phantom sketch

We compute intensity profile and universal quality index (UQI) in our method. The intensity profile represents the intensity scale of phantom image and reconstructed image. UQI index is defined as follows:

$$UQI = \left(\frac{2\mu\mu_r}{\mu^2 + \mu_r^2}\right)\left(\frac{2Cov(f, f^r)}{\sigma^2 + \sigma_r^2}\right) \quad (11)$$

where μ_r and μ represent the mean pixel values of two images, σ_r and σ are the standard deviations of the pixel values of two images, and $Cov(f, f^r)$ is the covariance between two images. It can be shown that the closer a reconstructed image to the reference one, the higher the quantity of UQI. UQI criterion reaches its maximum value 1.0 when the reconstructed image is identical to the reference image.

(1) Direct reconstruction

We use FBP algorithm to reconstruct the images under spectrum of 80/140kVp directly. Dimension of the images is 256×256. Due to the limit of space, we only show the results under spectrum of 80kVp in Fig.2, the UQI index is 0.9953. The intensity profile in the row of 128 is plotted in Fig.2 (c), the red curve shows the intensity scale of the phantom image, and the blue curve shows the reconstructed image. The description of the intensity profile is also applied to the following results.

(a) (b) (c)

Fig.2 Spectrum of 80kVp：(a) Phantom image (b) Reconstructed image
(c) Intensity profile (Row=128)

The results show that the reconstructed images at high-and low-energy levels are close to the phantom images which illustrate the model is reasonable and effective.

(2) Basis material density image

The water/iodine as basis material pair would generate a water density image and iodine density image, which can be used to judge the presence or absence of enhancement within a lesion. The results (in unit of g/cm^3) are as Fig. 3.

(a) (b)

Fig.3 Density image of basis material：(a) Water image (b) Iodine image

(3) Monochromatic image

Due to the limit of space, we only show the example monochromatic images at energy 70keV in Fig.4, the UQI index is 0.9957.

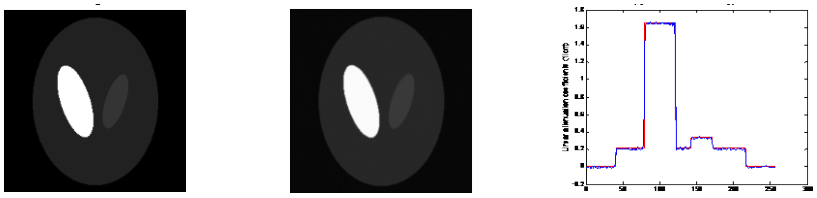

(a) (b) (c)

Fig.4 $E = 70keV$： (a) Phantom image (b) Monochromatic image
(c) Intensity profile (Row=128)

The reconstructed image is close enough to the phantom image at different energy level and it has a higher image contrast at low energy level but less beam hardening artifacts at high energy level which can be seen intuitively from the results.

(4) Electron density image

A series of articles showed that using ρ_e and Z_{eff} benefits radiotherapy applications where tissue characterization in terms of density or composition is desirable. The reconstructed results are shown in Fig.5, the UQI index is 0.9961.

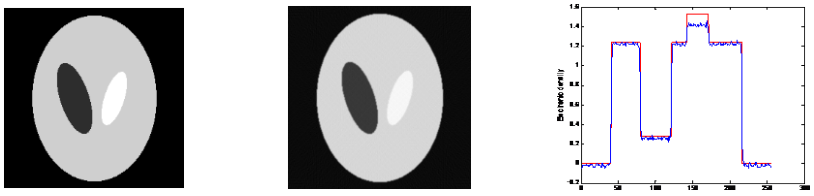

(a) (b) (c)

Fig.5 Electron density image：(a) Phantom image (b) Reconstructed image
(c) Intensity profile（Row=128）

We can see the reconstructed electron density image has some noise especially in the part of B-100 which represents the human bone, and the image intensity of the other parts is close enough to the phantom image intensity.

(5) Effective atomic number image

The reconstructed effective atomic number image is shown in Fig.6, the UQI index is 0.9861.

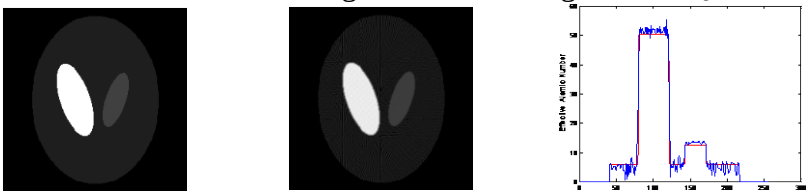

(a) (b) (c)

Fig.6 Effective atomic number image：(a) Phantom image (b) Reconstructed image (c) Intensity profile（Row=128）

From Fig.6 (b) we can see that the reconstructed image has some clearly noise and Fig.6 (c) presents clearly non-uniform distribution.

4. Discussions and Conclusion

The error contained in the experimental results, especially for the electron density image and the effective atomic number image, is an issue for our method. The main possible reasons for the error are summarized as below. Firstly, the process of computing electron density or effective atomic number has certain approximation in principle. Secondly, the atomic number of the object material is between the atomic number of basis materials or near one of them, the decomposition error will be small, otherwise the error is large [3]. According to the parameters obtained from NIST standard database, we find that the physical characteristics of basis materials (water/iodine) is similar to A-150 and diluted iodine, which means B-100 is greatly different from basis materials that may cause errors in the part of B-100 for the reconstructed results.

A method to realize the numerical simulation for the material decomposition and image reconstruction of DECT imaging is proposed in this paper. The experimental results show the validity and the reliability of our method. We believe it is beneficial for those theoretical researchers of DECT imaging domain.

Acknowledgements

This work is supported by the National Nature Science Foundation of China under the grant 61071053, and the Nature Science Foundation of Shandong Province under the grant ZR2014FM006.

References:

[1] Primak A N, Giraldo J C R, Eusemann C D, et al. Dual-source dual-energy CT with additional tin filtration: Dose and image quality evaluation in phantoms and in-vivo[J]. AJR. American journal of roentgenology, 2010, 195(5): 1164.

[2] Zhang D, Li X, Liu B. Objective characterization of GE discovery CT750 HD scanner: gemstone spectral imaging mode[J]. Medical physics, 2011, 38(3): 1178-1188.

[3] Zhang G, Cheng J, Zhang L, et al. A practical reconstruction method for dual energy computed tomography[J]. Journal of X-ray Science and Technology, 2008, 16(2): 67-88.

[4] http://sourceforge.net/projects/spectrumgui/.

[5] http://www.nist.gov/pml/data/xraycoef/index.cfm.

[6] Joshi M, Langan D A, Sahani D S, et al. Effective atomic number accuracy for kidney stone characterization using spectral CT[C]//SPIE Medical Imaging. International Society for Optics and Photonics, 2010: 76223K-76223K-12.